Ceramics International 42 (2016) 12283–12288

Contents lists available at ScienceDirect

Ceramics International

journal homepage: www.elsevier.com/locate/ceramint

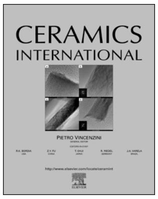

Influence of Mn-substitution on the structure and low-temperature electrical conduction properties of $PrCoO_3$

Heng Wang [a,b], Guangshe Li [a], Liping Li [a,*]

[a] Key Laboratory of Optoelectronic Materials Chemistry and Physics, Fujian Institute of Research on the Structure of Matter, Chinese Academy of Sciences, Fuzhou 350002, PR China
[b] College of Science, Guilin University of Technology, Guilin 541008, PR China

ARTICLE INFO

Article history:
Received 15 February 2016
Received in revised form
28 March 2016
Accepted 29 April 2016
Available online 30 April 2016

Keyword:
Perovskite oxide
Electrical transport
Infrared spectra
Impedance spectroscopy

ABSTRACT

Rare earth cobalt perovskite oxide ($LnCoO_3$) is one kind of complex metal oxides and has a wide variety of applications. The performance of $LnCoO_3$ is controlled by its electrical conduction, and therefore it is essential to study the behaviour of electrical conduction in $LnCoO_3$ and elucidate the corresponding conduction mechanism. In this work, a series of $PrCo_{1-x}Mn_xO_3$($x = 0, 0.05, 0.1, 0.15, 0.2$) were prepared by sol-gel method. The structures and low-temperature electrical conduction properties of these samples were investigated using x-ray diffraction, infrared spectra and alternating current impedance spectroscopy. All samples crystallized in an orthorhombic perovskite structure. Structural refinements reveal that the lattice parameters increased, while the orthorhombility decreased with Mn substitution. Further investigation of infrared spectrum indicates that the stretching vibration bands of Co-O bonds shifted towards lower wavenumbers followed by an increase of the population of Co^{3+} ions with intermediate spin state. These variations led to a reduced bandwidth of e_g band which could be the dominant reason for the abrupt decrease of bulk semi-conduction and the increase of activation energies for small polaron hopping conduction in $PrCo_{1-x}Mn_xO_3$.

1. Introduction

Rare earth cobalt perovskite oxides formulated by $LnCoO_3$ (Ln = rare earth ions) have found many significant applications such as cathodes materials for solid state oxide fuel cells [1], thermoelectric materials [2,3], and catalysts [4,5] primarily due to their rich exotic physical properties as featured by insulator-metal transition (IMT) [6] and magneto-electronic phase separation [7]. Previous research showed that these special properties observed in $LnCoO_3$ are closely related to the complex nature of the spin degeneracy of Co^{3+}. For instance, Co^{3+}in $LaCoO_3$ exhibits a gradual crossover from low spin state (LS, $t_{2g}^6e_g^0$) to higher spin state (IS, $t_{2g}^5e_g^1$ or HS, $t_{2g}^4e_g^2$) around 80 K due to the comparable energies between the crystal field split and Hund exchange [8]. Similar behaviours have also been observed for oxides with smaller Ln^{3+} ions, while their transition temperatures are much higher. These phenomena are resulted from the increased crystal field splitting energies as induced by the contraction of lattice cell [9]. As a consequence, the properties of $LnCoO_3$ oxides are sensitive to the ionic radius of Ln^{3+}, mainly due to the structural distortion induced by space filling in perovskites lattice. The criterion of structural distortion is the tolerance factor as defined by the equation, $t = (R_A + R_O)/\sqrt{2}(R_B + R_O)$, where R_A, R_B, and R_O are the ionic radius for A site, B site, and O ions at ambient condition, respectively. The cubic structure could be stable when t is closer to unity. Generally, a smaller t value ($0.75 < t < 1.0$) is popular for practical perovskites, in which some structural distortions are found. It has been demonstrated experimentally and theoretically that BO_6 octahedra tilt to reduce the space group symmetry to alleviate chemical stresses at a smaller t factor [10]. The most noticeable features are the connections between the adjacent octahedral characterized by the bond angle of B-O-B, which is usually described by the inter-atomic interactions between d electrons on the neighboring transition-metal ions. Firstly, the bond angles of B-O-B are directly related to magnetic super-exchange interaction that determines the magnetic properties. In fact, the reduction of Neel temperature T_N has been observed in an antiferromagnetic orthorhombic perovskite as the angle deviates from 180° [11]. Secondly, the single electron bandwidth of e_g band W originated from the orbital hybridization between p-d electrons would reduce [12]. This could trigger a decrease in the mobility of charge carriers, and further the electronic conductivity. Besides, aliovalent doping for $Ln_{1-x}A_xCoO_3$ (A is the alkaline-earth ion) shows a rich phase diagram [13], such as those from paramagnetic insulator to the

---

* Correspondence author.
E-mail address: lipingli@fjirsm.ac.cn (L. Li).

http://dx.doi.org/10.1016/j.ceramint.2016.04.175
0272-8842/

ferromagnetic metal. The system is inhomogeneous, including both of ferromagnetic and antiferromagnetic correction.

Despite of the majority of the studies focusing on A-site doping, the influence of B-site doping on the structural and physical properties have received less attention [14–16]. Firstly, B-site elements could strongly affect the electrical conduction and magnetic properties of perovskite oxides. For example, $LaMnO_3$ and $LaFeO_3$ are antiferromagnetic insulators [17]; $LaCoO_3$ is nonmagnetic insulator; whereas $LaNiO_3$ is metallic [18,19]. Ni substitution at Co site could induce glassy ferromagnetism, magneto resistance and IMT in $LaCoO_3$ [20]. Substitution of nonmagnetic elements Al and Ga at B-site leads to the spin state transition of Co^{3+} because of the increased strength of covalence of Co-O bond in this system [21]. Secondly, for A-site doping, the chemical stresses would be alleviated by the tilting of BO_6 octahedra where the average B-O bond length has no change [22,23]. However, for B-site doping, it could directly distort BO_6 octahedra and change the average length of B-O bonds, and further tailor the interactions between *p-d* electrons and the single electron bandwidth as well. Therefore, with B-site doping, it is anticipated that new magnetic and electrical conduction properties of $LnCoO_3$ could be accessible.

In this study, polycrystalline materials $PrCo_{1-x}Mn_xO_3$ ($x = 0$, 0.05, 0.1, 0.15, 0.2) were prepared using a facile sol-gel method. The influence of Mn substitution on the structure and low-temperature electrical properties was investigated. The conductivity was precisely determined by the alternating current impedance spectroscopy. The bulk conduction behaviours were obtained through excluding the impact of grain boundaries which could be non-negligible at low temperatures, leading directly to the intrinsic features of the electrical transport in $PrCo_{1-x}Mn_xO_3$. All the conduction and infrared spectra were interpreted in terms of the single electron bandwidth associated with the structure distortion.

2. Experiment section

2.1. Sample preparation

All reagents employed in the experiments were of analytical grade and used without further purification. According to the nominal formula of $PrCo_{1-x}Mn_xO_3$ ($x = 0$, 0.05, 0.1, 0.15, 0.2), all samples were prepared using a sol-gel method. In a typical preparation process, appropriate amounts of Pr_6O_{11} were dissolved in diluted HNO_3 to form a given concentrated $Pr(NO_3)_3$ solution. Excess HNO_3 was removed by evaporation in the fume cupboard. $Co(NO_3)_2$ was dissolved in the deionized water to form aqueous solution. 50 wt% $Mn(NO_3)_2$ aqueous solution was employed. The above three solutions were fully mixed and then added into the citric acid aqueous solution. The molar ratio of the citric acid to metal ions was set at 2:1. Then, ethylene glycol was added to form a stable sol. The molar ratio of ethylene glycol to citric acid was set at 2:3. After stirring for 3 h at room temperature, the above sol was evaporated at 70 °C in a constant temperature bath to get the transparent viscous gel. The obtained gel was heated at 150 °C for 15 min and then 300 °C for 3 h to get the black precursor. Finally, the precursor was heated at 900 °C for 8 h to obtain the sample powder.

2.2. Sample characterization

Crystal structures of the samples were determined by X-ray diffraction (XRD) on a Rigaku DESKTOP X-ray diffractometer using a copper target. XRD patterns were collected in the 2θ range from $20°$ to $85°$ with a step of $0.02°$ and a counting time of 8 s per step. Ni powder was served as the internal standard for peak positions calibration. The vibrational properties of the samples were measured using infrared spectra on a Perkin-Elmer Spectrum One spectrometer in the range of 400–4000 cm^{-1} at a resolution of 4 cm^{-1} using a KBr pellet technique after diluting the samples in KBr. The weight ratio of the samples to KBr is set at 1%.

2.3. Electrical property evaluation

Electrical conductivities of the samples were measured using the alternating current impedance spectra. Samples with the given quantity were mixed with 4% PVB (poly (vinylbutyral)), and then pressed uni-axially into pellets with a diameter of 7 mm and about 2 mm in thickness. The pellets were calcined at 500 °C for 2 h to remove the rudimental PVB and 1200 °C for 10 h to get the final ceramic pellets. Silver paste was painted onto both sides of the pellets as electrodes. To obtain an excellent contact between silver electrodes and pellet, the painted pellets were annealed at 600 °C for 2 h before conductivity test. Alternating current impedance measurements were performed using impedance analyser (Agilent 4294 A) in the frequency range of 40 Hz to 5 MHz from 100 K to room temperature with an oscillation voltage of 500 mV. The logarithm scanning way was used in the present frequency region. All measurements were carried out in air. The impedance data were analysed by an equivalent circuit model using the program of Zsimpwin (PerkinElmer Instruments).

3. Result and discussion

3.1. Phase and structure

Fig. 1(a) shows XRD patterns of $PrCo_{1-x}Mn_xO_3$ ($x = 0$, 0.05, 0.1, 0.15, 0.2) obtained after sintering at 1200 °C for 10 h. All XRD data could be indexed to the single orthorhombic perovskite phase (space group: *Pnma*). The lattice parameters were calculated by Rietveld refinement using GSAS program [24]. Fig. 1(b) gives the Rietveld refinement profile of $PrCo_{0.9}Mn_{0.1}O_3$. Fig. 2(a) shows the lattice parameters *a*, *b*, *c*, and cell volume *V* as a function of the contents of Mn ions. It is seen that all lattice parameters, *a*, *b*, *c*, and cell volume *V* increased with increasing Mn content. Here, both the valence and spin states of two ions should be considered. Firstly, it was demonstrated that the valences of Co and Mn ions in this system were +3, although a small amount of Mn^{4+} may be present due to the oxidation of Mn^{3+} in air [25]. Secondly, Mn^{3+} ($3d^4$) exhibited a high spin state (HS). However, the spin state of Co^{3+} ($3d^6$) in $PrCoO_3$ is much more complicated and even debated. Usually, low spin state (LS) is expected below 200 K, which exhibits a gradual crossover to HS or intermediate spin state (IS) with increasing temperature [26,27]. At room temperature, the mixing of the LS and HS (or IS) could be expected. The ionic radius of Mn^{3+} (HS) in 6-fold coordination is 0.645 Å, while that for Co^{3+} (HS) is 0.61 Å. Although the ionic radius of Co^{3+} (IS) is unknown, it could be smaller than that of Co^{3+} (HS) and Mn^{3+} (HS). Therefore, when larger Mn^{3+}ions are incorporated into Co^{3+} sites to form the solid solutions $PrCo_{1-x}Mn_xO_3$, the cell volume would increase. Table 1 lists the structure information, including the bond distances of Co-O(1), Co-O(21), and Co-O(22), average distance d_{av}, and bond angles θ_{av} in $PrCo_{1-x}Mn_xO_3$. It is seen that the value of d_{av} consistently increased with Mn^{3+} doping. This increase further affects the vibration of Co-O bonds, which will be analysed in the following IR spectra. It is worth mentioning that the variation of Co-O bond length with Mn^{3+} doping is distinctly different from that observed for A-site doping situation. For the latter case, the length of Co-O bonds maintains a constant due to the rotation of CoO_6 octahedra as indicated by the decreased Co-O-Co angles [22,23,28]. In order to estimate the symmetry of the system, the axis aspect ratio and the orthorhombicity were also calculated, as showed in Fig. 2(b). Both *c*/*a* and *b*/*a* values were decreased with